



Article

Dynamic Modelling of Enzymatic Hydrolysis of Oil Using Lipase Immobilized on Zeolite

Aysha Al Qayoudi ¹ and Sulaiman Al-Zuhair ^{1,2,*}

¹ Chemical and Petroleum Engineering Department, United Arab Emirates University, Al Ain 15551, United Arab Emirates; 201304543@uaeu.ac.ae

² National Water and Energy Center, United Arab Emirates University, Al Ain 15551, United Arab Emirates

* Correspondence: s.alzuhair@uaeu.ac.ae; Tel.: +971-37135356

Abstract: Immobilization has been proposed as a way to simplify the separation and repeated reuse of enzymes, which is essential for their feasible application at industrial scales. However, in their immobilized form, enzyme activity is fully utilized, due primarily to the additional diffusion limitations. Here, the immobilization of lipase on zeolite and its use in catalyzing oil hydrolysis is studied. Adsorption isotherms were investigated, and the data identified the model that best describes the process, which is the Sips model. The adsorption capacity of zeolite was determined as 62.6 mg/g, which is relatively high due to the high porosity of the support. The rate of enzymatic hydrolysis of olive oil, using the immobilized lipase, was determined at a pH of 7 and a temperature of 40 °C and was compared to that when using free enzymes. The results determined the parameters for a diffusion-reaction model. The effects of both the surface reaction and diffusion were found to be significant, with a slightly higher effect from surface reactions.

Keywords: lipase; immobilization; zeolite; oil hydrolysis; diffusion-reaction model



Citation: Al Qayoudi, A.; Al-Zuhair, S. Dynamic Modelling of Enzymatic Hydrolysis of Oil Using Lipase Immobilized on Zeolite. *Sustainability* **2022**, *14*, 8399. <https://doi.org/10.3390/su14148399>

Academic Editor: Shashi Kant Bhatia

Received: 13 June 2022

Accepted: 7 July 2022

Published: 8 July 2022

Publisher's Note: MDPI stays neutral with regard to jurisdictional claims in published maps and institutional affiliations.



Copyright: © 2022 by the authors. Licensee MDPI, Basel, Switzerland. This article is an open access article distributed under the terms and conditions of the Creative Commons Attribution (CC BY) license (<https://creativecommons.org/licenses/by/4.0/>).

1. Introduction

Lipases are enzymes that have received increased attention as the premier group of biocatalysts for biotechnological applications [1]. Lipases are triacylglycerol hydrolases that are produced by several organisms, with the natural function of hydrolyzing fats and lipids. These can be produced and extracted from different sources, such as plants, animals, and micro-organisms, and their characteristics differ depending on the source and mode of production [2]. Lipases are increasingly used in a variety of industries, including: dairy, beverage, and food production; detergent production; pharmaceuticals; textile production; biodiesel production; the synthesis of fine chemicals; agrochemicals; new polymeric materials; fuel production; fat and oil production; pollution control; personal care and cosmetics production [1,2].

However, the use of enzymes in the industry faces many challenges, including low thermal and chemical stability and narrow operational pH and temperature ranges. The most important challenge that faces the commercial application of enzymes is their high cost [3]. Therefore, unless enzymes are easily recovered with maintained activities, allowing the effective reuse of the enzyme for several cycles, enzymatic processes would inevitably be unfeasible [3,4]. Therefore, it is necessary to find ways to improve the reusability and stability of enzymes. Different purification procedures have been used to separate and recycle soluble enzymes, including ultrafiltration, precipitation, liquid–liquid partitioning, and chromatography. However, these techniques are either time-consuming, have low productivity, or are expensive, making them all unsuitable for continuous processes [5]. Recently, an aqueous two-phase flotation system has been proposed, using a hydrophilic organic solvent and inorganic salt recycling [6]. The main drawback of this process is its harmful environmental impact, which was overcome by the complete recycling of the

two phases [6]. The more practical approach for the industrial application of high-cost enzymes that has gained the most attention is enzyme immobilization. Using the enzymes in immobilized form allows their easy retention and repeated use in continuous reaction systems, which results in a decreased overall cost of the process. Enzyme immobilization, which is the attachment of enzyme molecules to solid supports [7], has been proposed for better reusability by improving enzyme stabilization, as it has been reported to enhance the enzymes' thermal and shear stability [8], as well as simplifying the separation [7]. Furthermore, immobilization inside a porous support could protect enzyme molecules from exposure to harsh media. In this regard, zeolites appear to be excellent supports for protein immobilization, owing to their low density and crystalline microporous aluminosilicates [9]. They also have excellent properties, such as a high ion-exchange capacity, strong acidic sites, a large surface area, and high thermal and mechanical stabilities [10,11]. Furthermore, zeolites, specifically the Cu/NaY zeolite, were recently shown to have a high adsorption capacity toward proteins [12]. Using a standard protein as an adsorbate, namely, bovine serum albumin (BSA), the adsorption capacities of NaY zeolite were found to be 84.61 mg/g.

In this work, the adsorption of lipases on zeolite was investigated. Lipases from *Eversa Transform 2.0* were used, which are reported to have higher thermal stabilities and lower sensitivities to the presence of phosphate anions than other lipases [13]. The immobilization capacity and activity of immobilized lipases are considered. The ability of zeolite to immobilize lipases and the activity of the immobilized enzyme were tested. The data helped to develop a mathematical model of the immobilized lipase for the simultaneous diffusion-reaction system. This kinetic model is very useful for understanding and forecasting the behavior of the system and can be used to optimize it. A valid model can also allow for the discovery and evaluation of improvement strategies, saving time and resources. Thus, one common use of models is to recommend methods that result in gains in the productivity and yield of the desired product. As far as the authors are aware, studying the adoption of lipase on zeolite and the dynamic of its reaction, similar to the one presented in this work, is currently lacking in the literature.

2. Materials and Methods

2.1. Chemicals and Enzymes

Zeolites (1.5 mm diameter granules and density of 0.61 kg/m³) were provided by JX-Nippon Research Institute (JX-NRI), Tokyo, Japan. Lipases from *Eversa Transform 2.0* were gifted from Novozymes, Bagsværd, Denmark. The olive oil was acquired from a local market and was used as a substrate. All additional reagents of analytical grade, including the Bradford reagent used for protein identification, were purchased from Merck, Readington Township, NJ, USA.

2.2. Enzyme Immobilization

Enzyme solutions of the different initial protein concentrations were prepared by diluting the stock enzyme solution in a phosphate buffer (2.0, 1.5, 1.0, 0.5, and 0.25% v/v) with 40 mL of the diluted enzyme solutions, mixed with 2 g of zeolite, in a 100 mL conical flask. The solutions were incubated in a water-bath shaker (Maxturdy-30; DAIHAN Scientific, Wonju, Korea) at 100 rpm and 25 °C for 24 h to reach equilibration. Subsequently, the mixture was centrifuged at 2000 rpm for 2 min to separate the zeolite. To measure the amount of adsorbed lipase on the zeolite, the protein content was measured in the initially prepared solution and the supernatant after removal of the immobilized lipases on the zeolite. The Bradford reagent was added to the samples and the absorbance values at 595 nm were measured using a spectrophotometer (BMG SPECTROstar, Ortenberg, Germany). By binding with the proteins in the solution, the maximum absorbance of Coomassie Brilliant Blue G-250 dye, found in the Bradford reagent, shifts from 465 to 595 nm. The absorbance values of solutions with different known concentrations of the standard protein albumin were recorded and used to develop a calibration curve, which

provided the protein concentrations in the samples. The equilibrium of adsorbed enzyme on the support was then determined using Equation (1):

$$q_e = \frac{(C_i - C_e)V}{m} \quad (1)$$

where q_e (mg/g) is the amount of enzyme adsorbed per g of solid at equilibrium, C_i and C_e (mg/mL) are the initial and equilibrium free enzyme concentrations in the supernatant, respectively, V (mL) is the solution volume, and m (g) is the weight of the adsorbent. The immobilization efficiency (IE) was determined from the ratio of enzymes attached to zeolite to the total available enzymes, as given by:

$$IE = \frac{(C_i - C_e)}{C_i} \times 100\%. \quad (2)$$

Several theoretical and empirical models were developed to represent the adsorption isotherms. However, no single model can completely describe all mechanisms and shapes. The most common models adopted in this work are the Langmuir, Freundlich, and Sips models, which are defined by Equations (3)–(5):

$$q_e = \frac{q_m b C_e}{1 + b C_e} \quad (3)$$

$$q_e = a_F F \cdot C_e^{1/n} \quad (4)$$

$$q_e = \frac{K_{LF} C_e^{n_{LF}}}{1 + (a_{LF} C_e)^{n_{LF}}}. \quad (5)$$

All models are semi-empirical, with temperature-dependent parameters having clear physical meanings. For example, q_m (mg/g) is the maximum adsorption capacity, b (mL/mg) is a solid energy constant related to the heat of adsorption, and $1/n$ is the degree of adsorption that describes the surface homogeneity. The Langmuir isotherm is the simplest and most common model to describe adsorption and can be effective when describing chemical adsorption. The adsorption in this model is assumed to be a monolayer, where a single layer of molecules is adsorbed on the adsorbent surface [14]. Therefore, the adsorbent surface is homogeneously structured, wherein all adsorption sites are identical, energetically equivalent, and uniform. There is no adsorbate transmigration in the surface stage. The Langmuir isotherms tend to fit the data better at higher concentrations. However, when the sorbate concentration is low, the effectiveness of the Langmuir model is reduced to a linear isotherm [15], which may not always be sufficient to describe the process.

On the other hand, the Freundlich isotherm model is an empirical equation that describes the non-ideal and reversible nature of adsorption and is applied to multilayer adsorption. The model predicts a heterogeneous adsorbent surface and active sites, with a non-uniform energy distribution for adsorption heat and affinities [16]. Freundlich isotherms tend to fit experimental data better at low concentrations; however, the main drawback of this model is that it deviates from Henry's law at low concentrations, which means that it lacks a fundamental thermodynamic basis [15,17].

Sips provided a model that combined both basic Langmuir and Freundlich isotherms in his advanced isotherm model [17]. This model is based on a heterogeneous adsorption system that is without adsorbate–adsorbate interactions. At sufficient concentrations, the resulting equation gives an expression with a finite limit [16]. This efficiently reduces to a Freundlich isotherm at low concentrations, which defies Henry's law, whereas the model predicts a monolayer sorption capacity following the Langmuir isotherm at high concentrations [15]. The Langmuir and Freundlich models are the monolayer adsorption isotherms that are most commonly used to fit adsorption experimental data using two adjustable parameters [18–21]. For the three-parameter monolayer adsorption isotherm models, the Sips model is regarded as the most appropriate [22].

2.3. Enzymatic Reaction Rate

The reaction rate at different substrate concentrations was determined for oil hydrolysis. Olive oil (selected as the model oil) has a high monounsaturated fatty acid content, the primary component being oleic acid (55–83%). Other fatty acids in olive oil are linoleic acid (2.5–21%) and palmitic acid (7.5–20%) [19]. The average molecular weight of the oil was determined from the average composition. An emulsifying reagent was first prepared for the stabilized substrate emulsion. The emulsifying reagent consisted of a glycerol solution in demineralized water (1:1 volume ratio) containing KH_2PO_4 and NaCl at concentrations of 0.4 and 17.9 mg/mL, respectively. Under continuous agitation using a magnetic stirrer (CB162, UK), gum arabic (6 mg/mL) was slowly added to form a homogenized mixture. To prepare the stable substrate emulsion, 20 mL of the emulsification solution was mixed with 2 mL of olive oil. Demineralized water was then added to bring the total volume to 100 mL and the solution was vigorously mixed. After stabilizing the substrate emulsion, serial dilutions (2.0, 1.5, 1.0, 0.5, and 0.25% *v/v*) were prepared in deionized water and the pH was adjusted to 7.0 by adding NaOH.

In Erlenmeyer flasks, 6.5 mL of neutralized substrate dilutions were combined with 1 mL of buffered enzyme solution (2.22 mg protein/mL) to initiate the hydrolysis reactions. To ensure a similar amount of protein was added when the immobilized lipase was used, 0.38 g of L-zeolite with a predetermined protein content of 5.85 mg protein/g was added, instead of the 1 mL solution of free enzymes. After incubating the mixture at 40 °C for 30 min, two drops of the phenolphthalein indicator were added. Titration against the 0.5 mM NaOH solution was performed until the color of the solution changed. Following the same procedure, an additional blank test was performed using 1 mL of distilled water instead of the 1 mL enzyme solution. The titrated volume of the NaOH solution required to neutralize the fatty acids produced by the enzymatic hydrolysis of the oil was recorded. The initial rate of the hydrolysis reaction, *v* (mg/mL h), was determined using Equation (6):

$$v = \frac{(V_1 - V_0) \times M_{\text{NaOH}} \times MW_{\text{FAA}}}{V \text{ } 0.5 \text{ h}} \quad (6)$$

where V_0 and V_1 are the volumes of NaOH used until the blank solution and enzyme test sample change color (mL), respectively, M_{NaOH} is the NaOH solution molarity (*M*) used, *V* is the volume of the reaction mixture (7.5 mL), and MW_{FAA} is the average molecular weight of free fatty acids in olive oil, which was determined from the fatty acid composition [23].

2.4. Characterization of L-Zeolite

A Fourier-transform infrared spectrometer (FT/IR-6300, JASCO, Easton, MD, USA) was used to examine the immobilization functional groups in all materials. The FTIR contained a high-intensity ceramic and halogen lamp IR source and a 45° Michelson/corner-cube mirror interferometer with auto-alignment, DSP control, and a sealed structure (KRS-5 window). The morphologies of the zeolite and L-zeolite were studied using images taken with a scanning electron microscope (SEM, JCM-5000 NeoScope, Tokyo, Japan). Before imaging, the samples were cleaned and gold-coated using an Auto Fine Coater (JFC-1600, Tokyo, Japan) to boost the specimen's conductivity. The pore-size distributions of zeolite and L-zeolite were determined using a pore-size analyzer (TriStar II 3020 Analyzer, Micromeritics Instrument Corporation, Norcross, GA, USA). The temperature was held at 77 K while measuring the surface area. The crystallinities of the zeolite and L-zeolite samples were determined using an X-ray diffractometer analyzer (XPERT-3 Philips, Amsterdam, The Netherlands). The X-ray study used copper as the anode material and was set at 40 mA and 45 kV. The step size was 0.013 nm, and the measurement peaks were $5^\circ < 2\theta < 50^\circ$.

3. Results and Discussion

3.1. Characteristics of L-Zeolite

3.1.1. FTIR Analysis

The Fourier-transform infrared spectroscopy (FTIR) spectra of empty zeolite and L-zeolite are shown in Figure 1a,b, respectively, compared to that of free lipase (Figure 1c). The infrared spectra were taken at wavenumbers of 500–4000 cm⁻¹ to indicate the major structural groups and features of zeolite. The broad intense band observed around 900–1100 cm⁻¹ represents the asymmetric stretching vibration of Si-O-Si, while the less intense band around 650–750 cm⁻¹ was caused by the Si-O-Si symmetric stretching vibration. The FTIR of the empty zeolite in Figure 1a matches well with the FTIR patterns and peak sizes of the alpha-zeolite [24]. The adsorption peaks of L-zeolite observed around 1600–1660 cm⁻¹ are assigned from the amide I band, corresponding to the C=N and NH stretching modes, respectively. These are characteristic of the protein primary structure, which confirms the attachment of protein into zeolite, as reported in the literature. A noticeable increase at the -OH broadband above 3000 cm⁻¹ was detected after protein immobilization, which further proves the successful adsorption of lipase into the zeolite crystals [25,26].

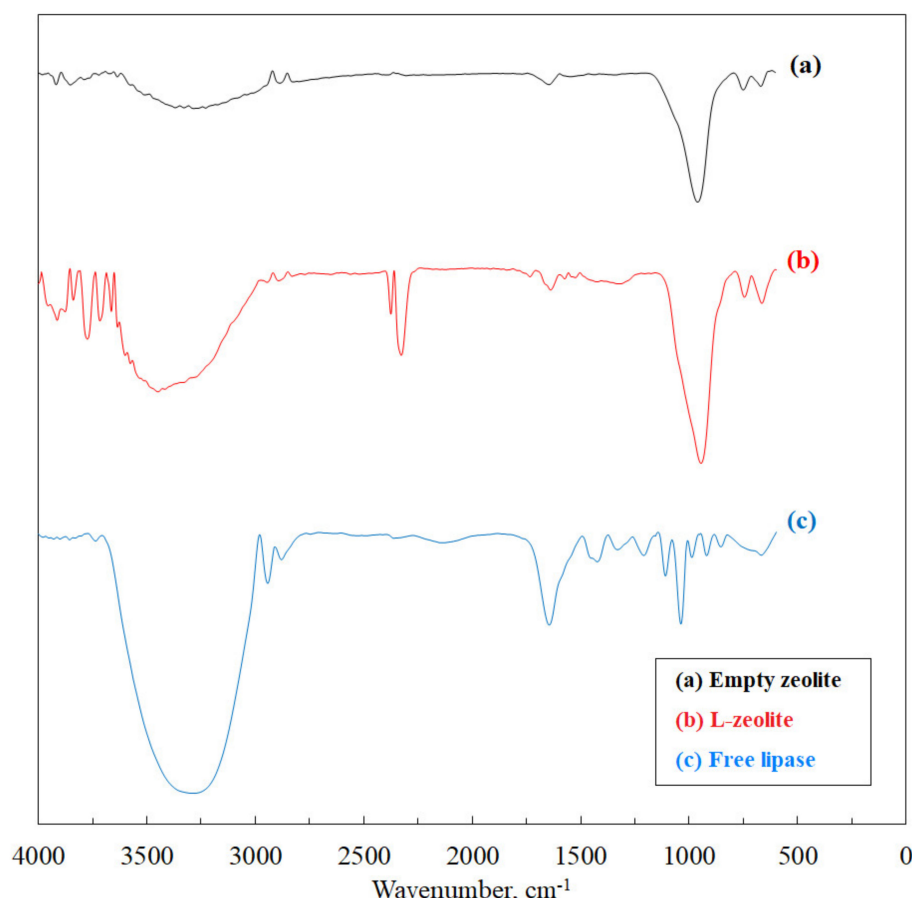


Figure 1. FTIR spectra of the (a) empty zeolite, (b) L-zeolite, and (c) free lipase.

3.1.2. XRD Analysis

The X-ray Diffraction (XRD) patterns of zeolite and L-zeolite are shown in Figure 2a,b, respectively. The pattern of the empty zeolite framework is similar to those reported in the literature [24,26]. With the lipase immobilization depicted in Figure 2b, a similar pattern to that of empty zeolite with no changes in the diffraction widths was observed, which indicates that the crystal sizes remained nearly the same. However, an intensity drop in the peaks was observed after lipase immobilization, which indicates a reduced crystal

sharpness. This change in the zeolite crystallinity with the attachment of lipase agrees with the SEM results presented in Section 3.1.3.

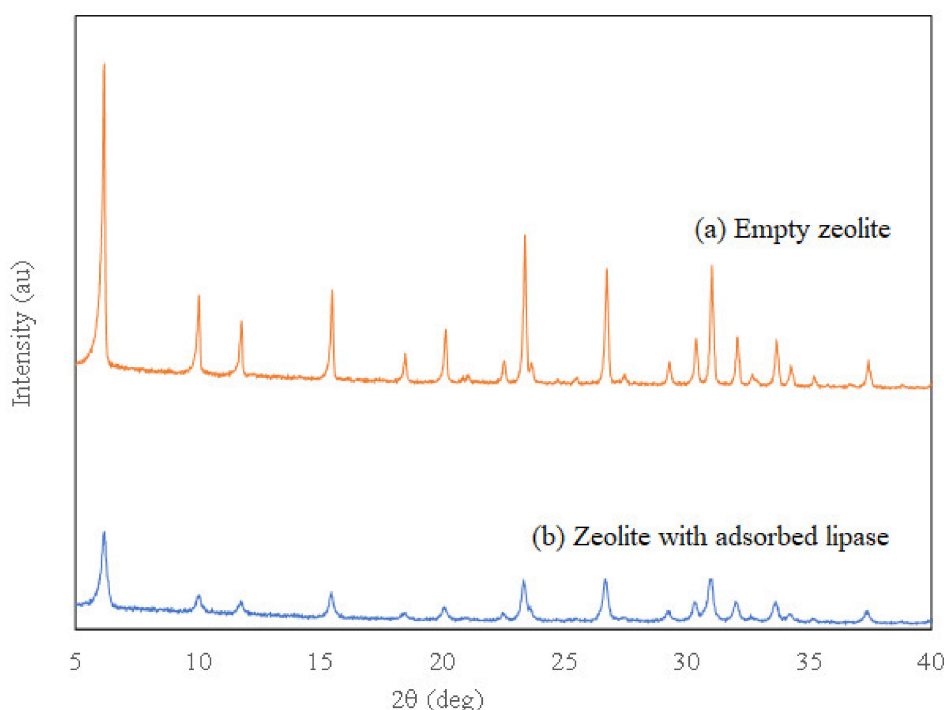


Figure 2. XRD image of the (a) empty zeolite and (b) the zeolite with adsorbed lipase.

3.1.3. Surface Morphology

The zeolite bead morphology was characterized before and after lipase immobilization using SEM, as shown in Figure 3a,b, respectively, at different image magnifications. The smooth surfaces of well-defined spherical structural crystallites were observed for the empty zeolite, which matches the reports in the literature [27]. With enzyme adsorption, the zeolite morphology maintains the same pattern, with no observed major difference in the crystal structure. Nevertheless, with enzyme immobilization, the surface becomes slightly rougher, with partial crystal clustering. This suggests that the enzyme molecules are attached to the outside surface of the zeolite.

3.1.4. Porosity and Surface Area

The N_2 adsorption–desorption isotherms at 77 K for empty zeolite and L-zeolite are shown in Figure 4a,b, respectively. The BET analysis was conducted, and the associated surface properties are shown in Table 1. The BET surface area of the empty zeolite was $361.37 \text{ m}^2/\text{g}$, which agrees with those reported in the previous literature [24]. With lipase immobilization, the surface area dropped to $107.93 \text{ m}^2/\text{g}$. The isotherm profile of zeolite was evaluated to be type I by following the IUPAC classification, exhibiting a sharp uptake in the low relative pressure region, which is a typical feature of microporous materials and also agrees with the results reported in the previous literature. A decreased BET surface area was observed after lipase adsorption, which is due primarily to the lipase molecules that occupy the pores. This further confirms the successful attachment of lipases. The pore size and volume were also found to decrease after lipase adsorption, from 1.805 nm and $0.227 \text{ cm}^3/\text{g}$ in empty zeolite to 1.800 nm and $0.081 \text{ cm}^3/\text{g}$ for L-zeolite, respectively.

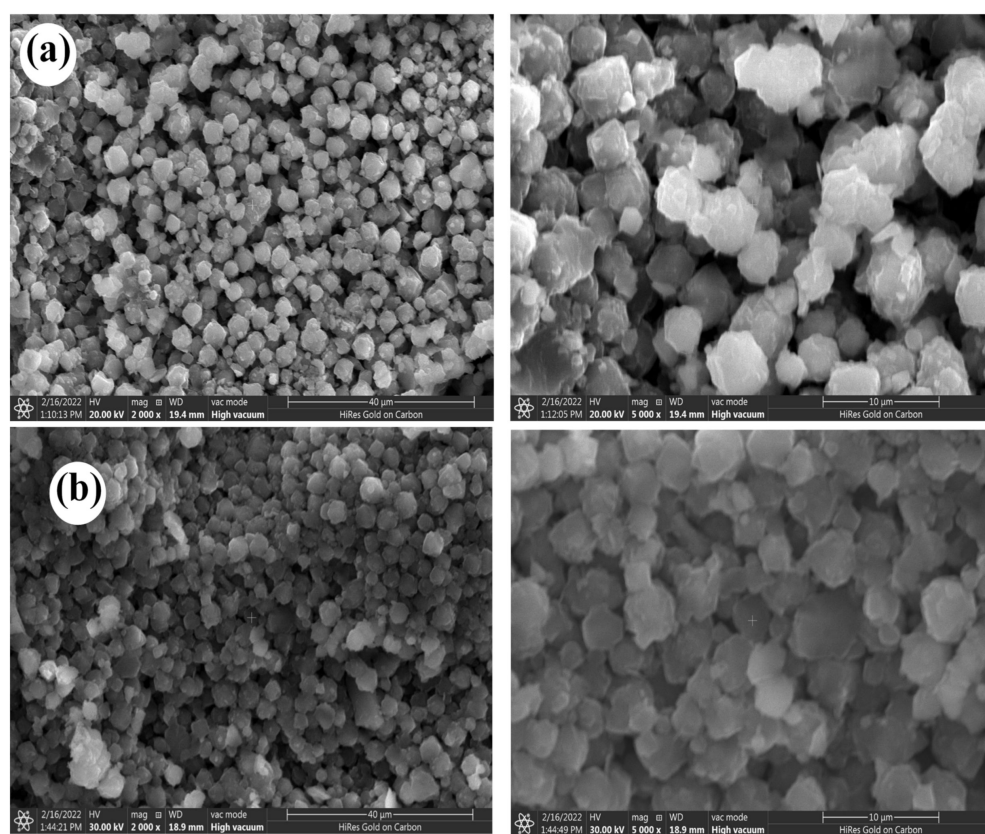


Figure 3. Scanning electron microscopy (SEM) images of (a) pure zeolite and (b) zeolite with adsorbed lipase, at different magnifications.

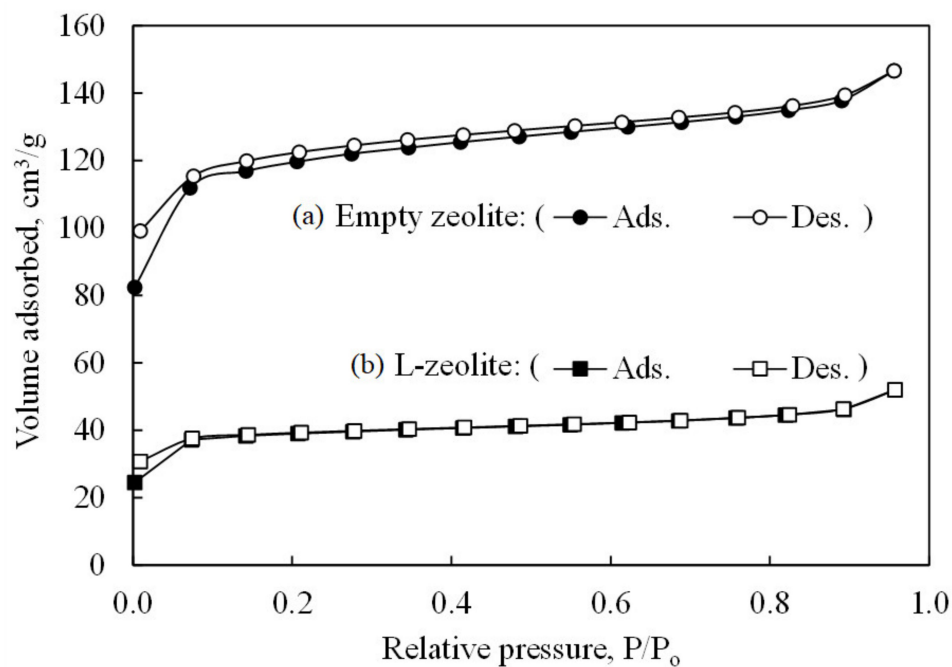


Figure 4. N_2 Adsorption isotherms at 77 K of (a) empty zeolite and (b) L-zeolite.

Table 1. BET surface area and pore characteristics of empty zeolite and zeolite with adsorbed lipase.

Composite	S_{BET} ($\text{m}^2 \text{ g}^{-1}$)	Total Pore Volume ($\text{cm}^3 \text{ g}^{-1}$)	Pore Size (nm)
Empty zeolite	361.37	0.227	1.805
L-zeolite	107.93	0.081	1.800

Figure 5 shows the pore-size distribution of empty zeolite and L-zeolite, in terms of the cumulative pore volume vs. pore size. The curves of the pore volume vs. the radius shown in Figure 5a indicate that larger-volume pores have larger sizes, with larger pore volumes for the empty zeolite at the same pore radius, compared with L-zeolite. The differential volume change vs. radius curves in Figure 5b shows that the highest differential change was at a radius of around 1.8 nm for both samples.

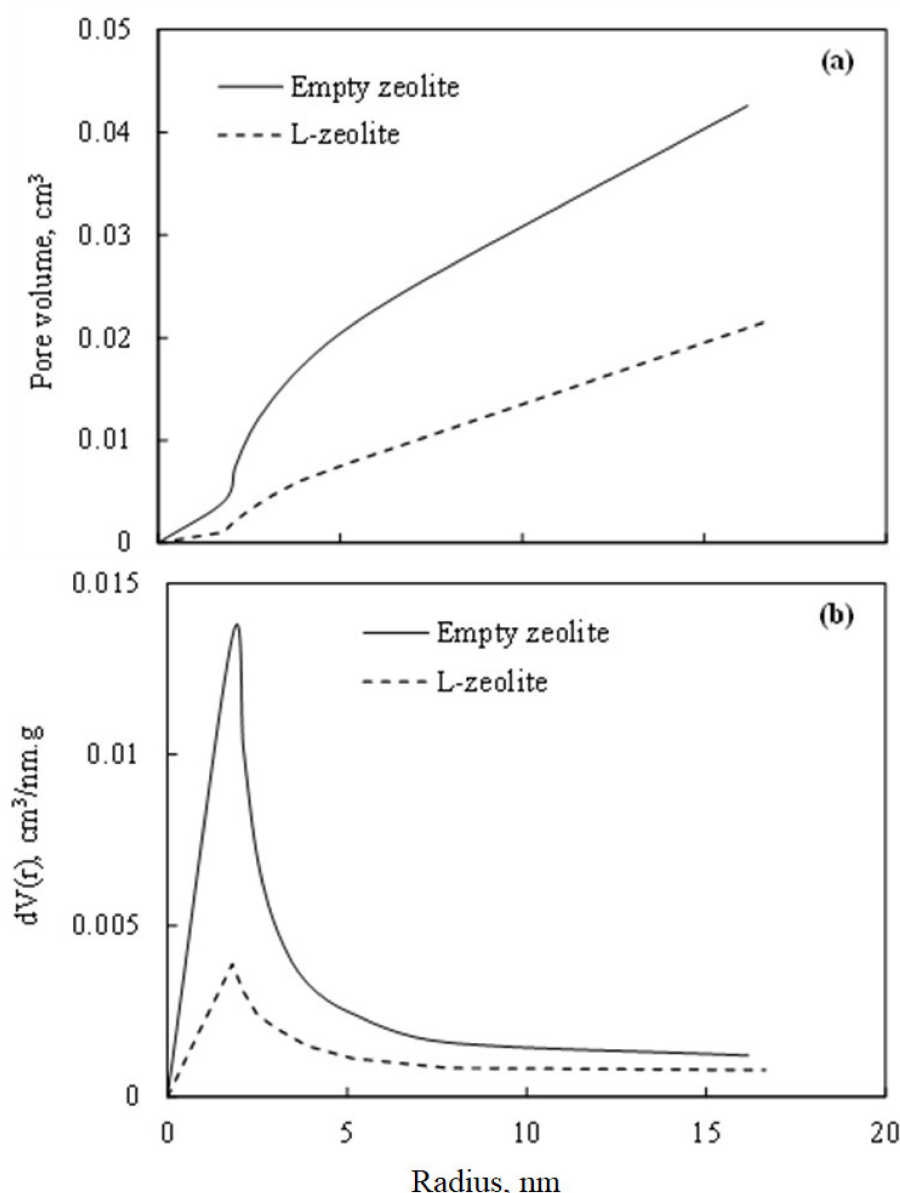


Figure 5. Pore size distribution of empty zeolite and L-zeolite: (a) pore volume vs. radius, and (b) differential volume change vs. radius.

3.2. Lipase Immobilization

3.2.1. Immobilization Efficiency

The amount of equilibrated enzyme adsorbed on zeolite was determined using enzyme solutions at different concentrations. To evaluate the IE, the ratio of enzymes attached to zeolite against the total available enzymes was determined, and the result is shown in Figure 6a. The IE initially increased with the initial concentration, which was the result of increasing the driving force of the enzyme diffusion into the internal pores of the zeolite. However, a reduced IE was observed as the initial concentration exceeded 1 mg/mL. This drop is primarily due to the limited capacity of the support surface. As the initial lipase concentration increases, the maximum capacity of the support surface is approached, and the effect of the increase in protein concentration on the increase in the surface capacity reduces, reaching a plateau, as shown in Figure 6b. Therefore, in this region, the IE, which is the ratio of the amount adsorbed (i.e., surface capacity) over the initial concentration drops. In other words, in this region, the increase in the nominator (amount adsorbed) is not less than the increase in the denominator (protein concentration), until a point where the nominator remains constant (when the maximum capacity is reached), while the denominator continues to increase.

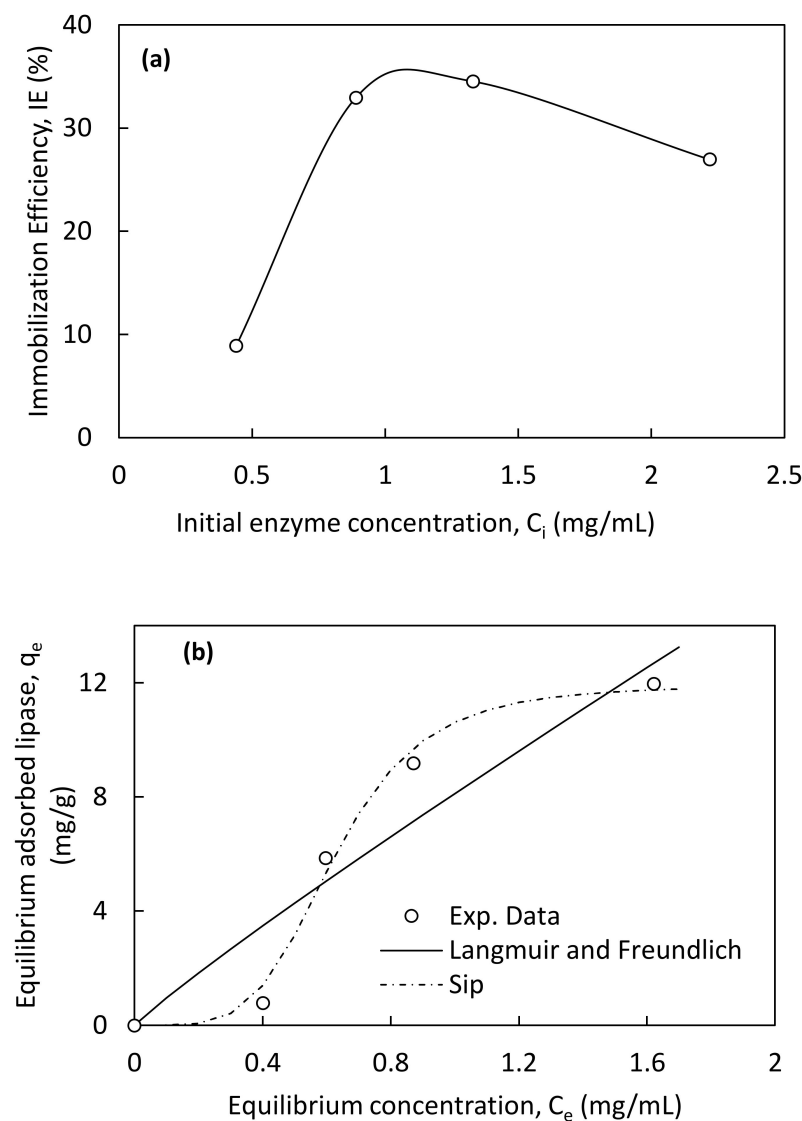


Figure 6. (a) Effects of the initial enzyme concentration on the immobilization efficiency (IE) and (b) adsorption isotherms of lipase adsorption on zeolite at 25 °C.

3.2.2. Adsorption Isotherms

The mathematical modeling of the adsorption equilibrium is essential to understanding the process and gaining better insight into the adsorption mechanism. This predicts the adsorption capacity, and also explains the properties of the adsorbent surface and its affinity toward the adsorbate [28,29]. Therefore, equilibrium data were fitted to three isotherm models (Langmuir, Freundlich, and Sips) via nonlinear regression, using the Polymath software. The estimated isotherm parameters and their corresponding coefficient of determination, R^2 , are presented in Table 2. The curves of the three models are compared to those of the experiments in Figure 6b. It should be noted that the Freundlich isotherm is drawn on the figure, but it is almost identical to the Langmuir and, hence, they are on top of each other. The Sips isotherm model was found to best describe the experimental data and trends, compared to the other two models, which is reflected in its greater coefficient of determination, as shown in Table 2. The Sips isotherm is a nonlinear combination of the Freundlich and Langmuir isotherms. The Sips model overcomes the limitations of an increasing adsorbate concentration with the Freundlich isotherm, which reduces to the Freundlich isotherm at low adsorbate concentrations. At high concentrations, it predicts a monolayer adsorption that is nearly identical to the Langmuir isotherm [30]. The good fit of adsorption isotherms by the Sips model reveals that the lipase adsorption creates the monolayer on the heterogeneous zeolite surfaces.

Table 2. Isotherm parameters for the Langmuir, Freundlich, and Sips models.

Isotherm	Parameters	Values	R^2
Langmuir	b	0.15	0.83
	q_m (mg/g)	62.58	
Freundlich	a_F	8.11	0.82
	n	1.08	
Sips (L-F)	a_{LF}	1.60	0.98
	K_{LF}	98.23	
	n_{LF}	4.51	

Table 3 shows the model parameters that best described the lipase adsorption on different supports; namely, sporopollenin, nylon-6, PA-M, ZIF-8, ZIF-67, HKUST-1, chitosan, and activated chitosan beads. Except for the activated chitosan beads, the adsorption isotherms of lipase on all other supports are best described using the Langmuir model. However, these studies did not consider the Sips model in their analysis. In addition, the data-skewing from the Langmuir model usually occurs at low adsorbate concentrations; hence, if this region is not tested, the significance of the Sips model may not be evident. Except for PA-M, the maximum adsorption capacity of zeolite was found to be 62.6 mg/g, which is higher but is of the same order of magnitude as the other supports. The lipase adsorption capacity of zeolite, as determined in this work, was slightly lower than the BSA capacity of Cu/NaY zeolite [12]. The high adsorption capacity of zeolite has also been reported in the literature [31,32], which is primarily due to its large surface area and high and uniform porosity [10,11]. Other external conditions, such as the pH and temperature, also affect the adsorption.

Table 3. Previously reported adsorption isotherm model parameters of lipase on different supports.

Support	Temp	Model Best Fit	Parameters	Values	R ²	Ref.
Sporopollenin	40 °C	Langmuir	b (mL/mg) q _m (mg/g)	0.76 13.47	0.952	[33]
Nylon-6	30 °C	Langmuir	b (mL/mg) q _m (mg/g)	11.641 1.793	0.997	[34]
PA-M	35 °C	Langmuir	K _L (mL/mg) q _m (mg/g)	21.2 253.2	0.994	[35]
ZIF-8	35 °C	Langmuir	K _L (L/mg) q _m (mg/g)	0.22 33.06	0.990	[36]
ZIF-67	30 °C	Langmuir	K _L (L/mg) q _m (mg/g)	6.76 34.22	0.873	[36]
HKUST-1	35 °C	Langmuir	K _L (L/mg) q _m (mg/g)	4.12 18.74	1.000	[36]
Chitosan beads	30 °C	Langmuir	b (mL/mg) q _m (mg/g)	797 0.158	0.946	[37]
Activated chitosan beads	30 °C	Freundlich	K _F (mL/mg) ^{1/n} 1/n	0.379 4.975	0.995	[37]

In addition to the structure, morphology, and size of the zeolite, acidity plays an important role in enzyme adsorption. By interacting with the acid sites on the crystalline surface, which are able to transfer protons from the solid to the adsorbed molecules, a zeolite acid is able to convert an adsorbed basic molecule into a conjugated acid form. In this chemical acid-base type of adsorption, the enzyme immobilization capacity increases with an increase in the acidity of the crystals, which in turn depends on the structure of the crystal's framework and its chemical composition. The main advantage of such chemical adsorption over physical adsorption is the high operational stability as a result of the stronger interaction, with a low level of leaching of the enzyme even if the process temperature, pH, or solvent are changed [38]. The main drawback of this attachment is the relatively lower initial activity, due to unfavorable conformational changes in the global structure of the enzyme or blockage of the active sites. The surface's hydrophobicity has also had a significant impact on both the activity and capacity of enzyme adsorption. The most popular supports for lipase immobilization are the hydrophobic ones because they sustain enzyme activity better than the hydrophilic supports. It was reported that lipase that was immobilized on a hydrophobic membrane exhibited an over 11-fold increase in activity compared to that exhibited by lipase immobilized on a hydrophilic membrane [39].

3.2.3. Diffusion-Reaction Kinetics Model

Enzymes generally bind to surfaces via weak bonds, such as those formed by hydrogen, electrostatic, van der Waals, and hydrophobic interactions [40]. Although these individual interactions have low energy, multipoint binding usually occurs, resulting in a relatively strong bond to the surface. The structure of the enzyme at the adsorbent surface may differ slightly from the original form but, generally, a considerable percentage of the native enzyme's activity is preserved.

The initial rate of hydrolysis reactions for olive oil using immobilized lipase on zeolite was determined at different substrate concentrations, as shown in Figure 7a. The experiments were repeated using free enzymes with the same amount of protein and under the same conditions. The results show that the rate of reaction for both free and immobilized enzymes increased as the olive oil concentration increased, with no observed substrate inhibition. However, the immobilized enzymes have a lower rate of reaction compared to free enzymes, which is primarily due to mass transfer limitations.

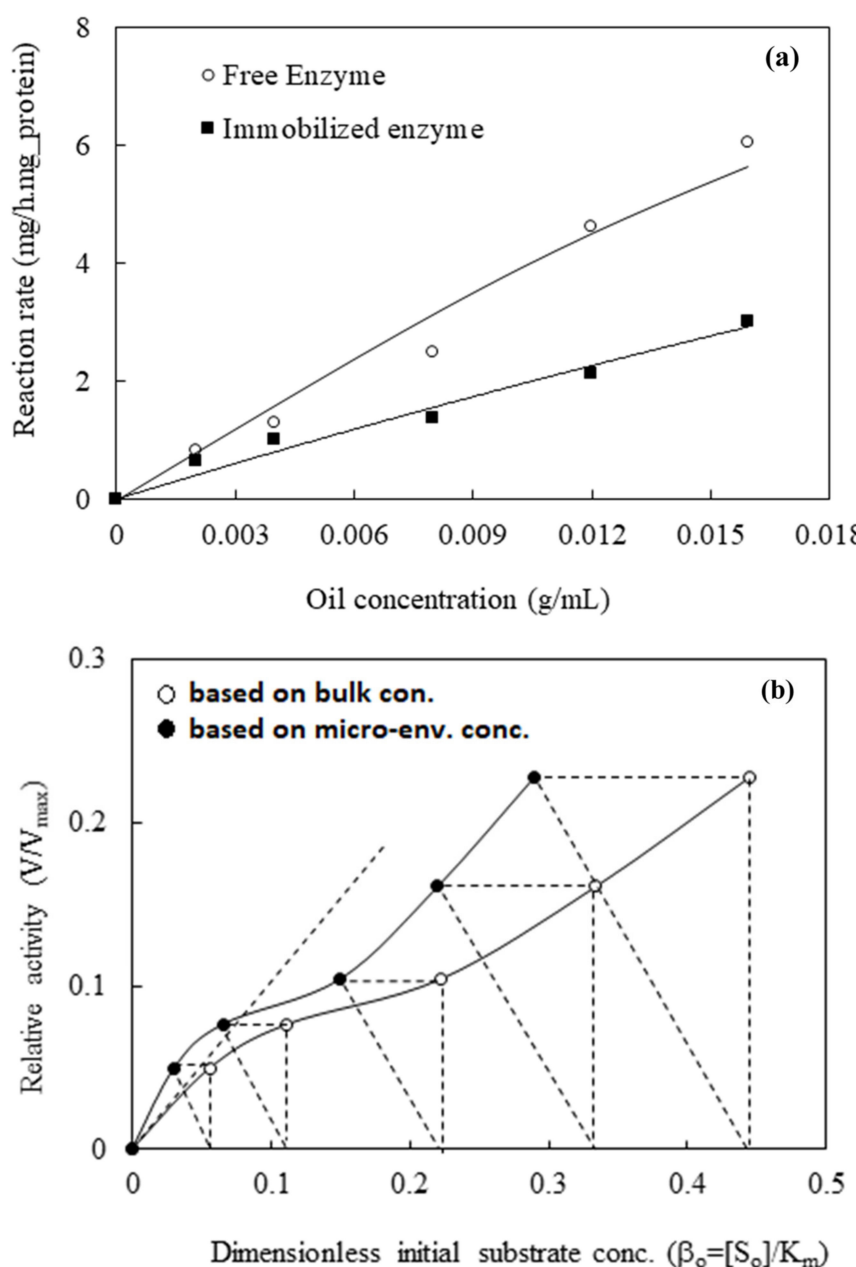


Figure 7. (a) Effect of the initial substrate concentration on the initial rate of oil hydrolysis, using free and immobilized lipases at 40 °C and 0.3 mg protein/mL of reaction with 0.38 g of the immobilized enzyme, and (b) a graphical determination of the enzymatic reaction rate in terms of the microenvironmental substrate concentration.

Assuming that the enzymatic reactions are described by Michaelis–Menten kinetics (Equation (7)), the reaction kinetic parameters were determined using the initial rate of reaction, v (mg/h·mg·protein), of the free enzyme, as shown in Figure 7a, using the Lineweaver–Burk method [41]:

$$v = \frac{V_{max}[S]}{K_m + [S]} \quad (7)$$

where V_{max} is the maximum reaction rate (mg/h·mg·protein), K_m (g/mL) is the Michaelis–Menten constant, which reflects the affinity of enzymes to the substrates, and $[S]$ (g/mL) is the substrate concentration.

The values of K_m and V_{max} were determined to be 0.036 g/mL and 15.2 mg/h·mg·protein, respectively, using the linear regression Lineweaver–Burk method, due to the initial rate of

oil hydrolysis with the free enzyme, as shown in Figure 7a. Table 4 compares the kinetic parameters from this work with other parameters, using free lipase from different sources in the hydrolysis of the same substrate used here (olive oil emulsion). The parameters using lipase from *Eversa Transform 2.0* were of the same order of magnitude as those found using lipase from *Rhizomucor miehie*. However, the V_{max} using *Eversa Transform 2.0* was higher. This was expected, as *Eversa Transform 2.0* is known for its higher activity compared to lipases from other natural resources. A higher value of V_{max} than that for the *Rhizomucor miehie* lipase was reported using porcine pancreas lipase. However, the value was still lower than in this work. The value of K_m was significantly lower than for *Eversa Transform 2.0*, which suggests a greater substrate affinity. This could be due to the use of smaller amounts of enzyme and olive oil emulsifications, which allows for better enzyme interactions [42]. The parameters using lipase from *Pseudomonas gessardii* were much lower than those reported in other studies [43]. These lower values could be caused by the reduced pH and temperature used, especially considering the fact that the pH was 3.5.

As protein adsorption on zeolite occurs only on the outer surface of zeolite [38], only external diffusion has been considered in this work. The relative activity (v/V_{max}) of the immobilized enzyme was mapped vs. the dimensionless bulk substrate concentration ($\beta_0 = [S_0]/K_m$) to estimate the reaction rate, based on the microenvironmental substrate concentration using the immobilized enzyme. Then, the mass transfer coefficient k_L was determined from the slope of the tangent line at time zero to be 1.02, as shown in Figure 7b. The intercept of the lines with a slope equal to $-k_L$, and the activity at each experimented point, were used to determine the rate of reaction, based on the microenvironmental substrate concentration.

The deposition of the by-product glycerol on the immobilized lipase could result in a drop in immobilized enzyme activity by obstructing the diffusion of the substrates and blocking the enzyme active sites. Since glycerol is hydrophilic, this effect can be reduced by employing a hydrophobic support. Additionally, compared to hydrolysis, the problem becomes more obvious during oil transesterification. This is due to the low solubility of glycerol in organic media, where transesterification takes place [44]. In order to reduce the impact of glycerol deposition, the by-product needs to be removed. The effectiveness of washing Novozym®435, a commercially available immobilized lipase B from *Candida antarctica* on a resin, with 1-butanol between the different cycles was confirmed via waste frying oil transesterification with methanol [45]. The enzyme was re-used for four consecutive cycles, without any activity loss.

Table 4. Kinetic parameters of enzymatic hydrolysis of olive oil using lipase.

Lipase Source	V_{max} (mg/h·mg·Protein)	K_m (g/mL)	Temp (°C)	pH	Ref
<i>Eversa Transform 2.0</i>	15.2	0.036	40	7.0	This work
<i>Rhizomucor miehie</i>	2.44	0.0553	37	7.0	[46]
<i>Porcine pancreas</i>	5.91	0.0042	37	6.9	[42]
<i>Pseudomonas gessardii</i>	0.01	0.0006	30	3.5	[43]

The predicted activity, developed from the immobilized enzyme results from the microenvironment concentration, was compared to the experimentally determined results using the free enzyme. The activity in the microenvironment represents the reaction rate at the surface of the support, i.e., without mass transfer limitations. This should be the same as those for the free enzyme at the same protein concentration. The results of the developed model were close to those using the free enzyme, as shown in Figure 8a, which verifies the model accuracy. A similar relative activity value of 0.3 was also reported on the hydrolyzed palm oil, using immobilized lipase on a hydrophobic Y-type zeolite [47]. The deviations between the two samples shown in Figure 8b indicate that there were no

significant differences at β_0 below 0.2. However, as the substrate concentration increased, the model predictions based on the microenvironment underestimated the reaction rate.

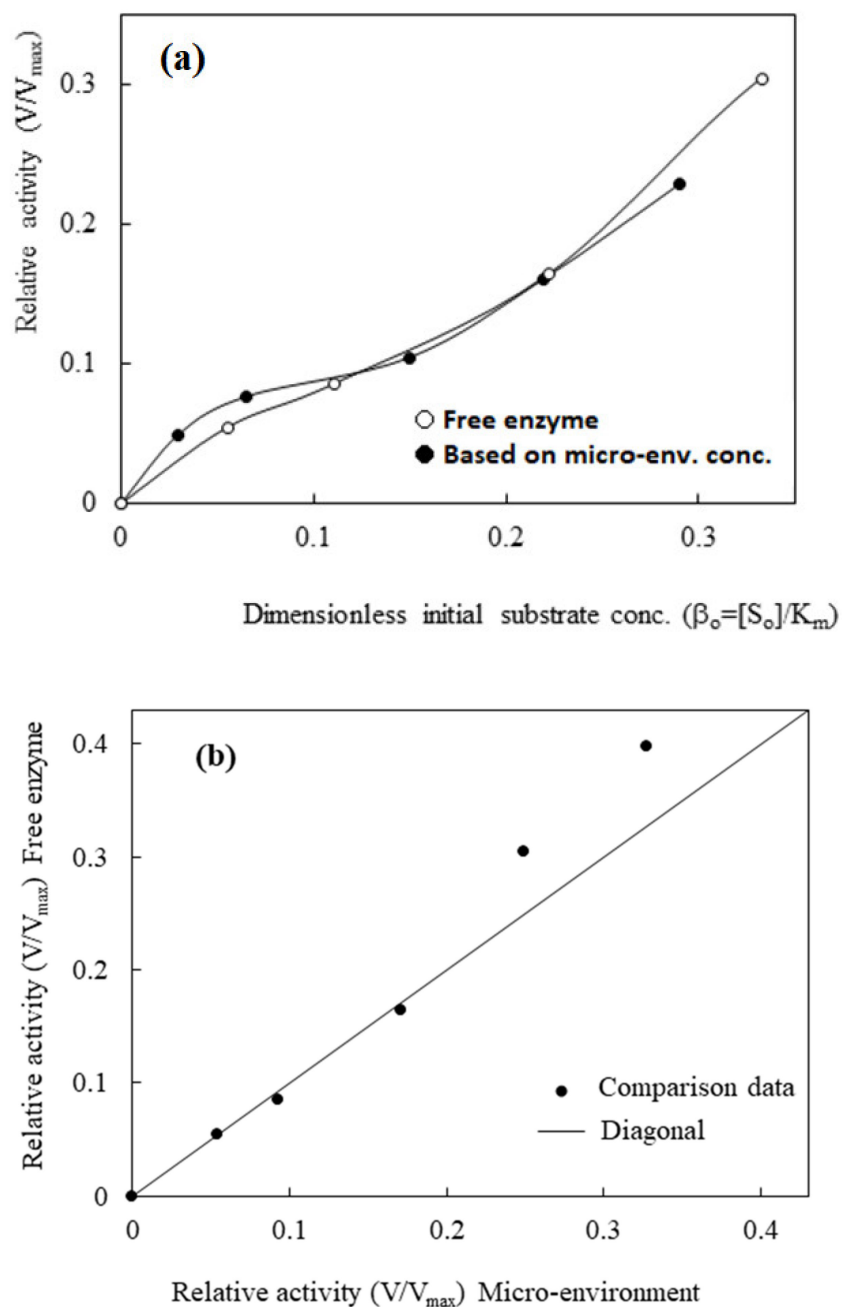


Figure 8. Comparison between enzyme activity based on the microenvironment substrate concentration and the experimental activity of the free enzyme. (a) Relative activity of free enzyme and that based on microenvironment vs. dimensionless initial substrate concentration, (b) Analysis of deviation between relative activity of free enzyme and that based on microenvironment.

The substrate modulus (μ) as defined by Equation (8), which is also known as the Damköhler number, is a dimensionless ratio that determines a measure of relative significance for the resistances, based on the surface reactions and external diffusion. High μ values indicate a more significant effect from the diffusion resistance, while lower values indicate a more significant effect from the surface reaction resistance. The determined μ for the enzymatic hydrolysis of olive oil using immobilized lipase on zeolite was determined

as 55.3, which suggests that both surface reactions and diffusion effects are significant, with a slightly higher effect from the surface reactions [46].

$$\mu = \frac{V_{max}}{K_L K_m} \quad (8)$$

This was also confirmed by the high values of the effectiveness factor, as defined by Equation (9), which relates the rate of reaction using free enzymes to that using immobilized enzymes, at the same protein amount and operating conditions. As shown in Figure 9, the effectiveness factor was consistently above 0.5 at the tested β_o values.

$$\eta = \frac{v}{v_{free}} \quad (9)$$

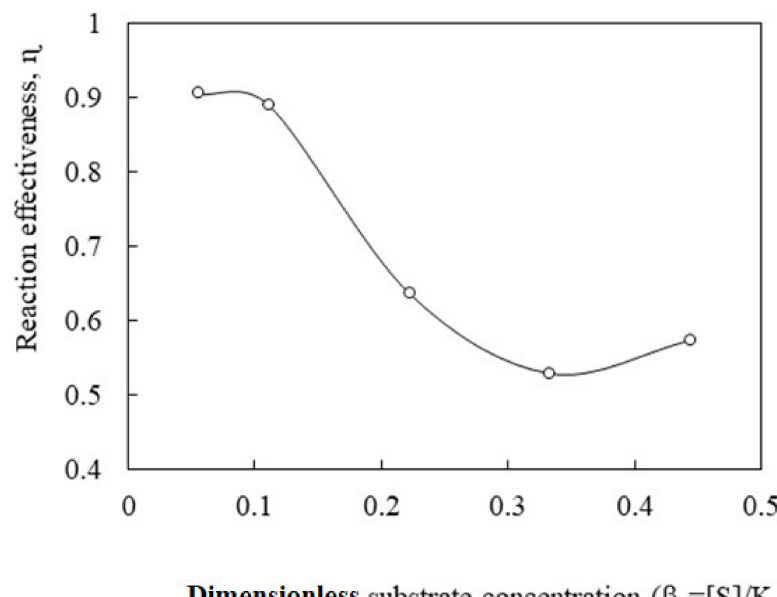


Figure 9. Effect of the substrate concentration on the reaction effectiveness factor.

Initially, the effectiveness dropped with an increased β_o , which could be attributed to the greater viscosity of the reaction system with the oil concentration. This increased viscosity negatively affects the diffusion efficiency and results in lower effectiveness. However, this effect is less significant for the increased diffusion driving force, with a greater bulk substrate concentration at β_o values above 0.35, and increased effectiveness was observed after that point.

4. Conclusions

Lipase was successfully immobilized on zeolite via adsorption. The adsorption was validated, and adsorption equilibrium was found to be best described by the Sips model. The SEM and XRD results showed no significant changes in the morphology and structure of zeolite with lipase adsorption. A developed diffusion-reaction dynamic model was used to describe the enzymatic hydrolysis of olive oil from immobilized lipase on zeolite. A good level of agreement was shown between the model predictions based on the microenvironment and the experimental results using free enzymes. These results provide valuable information on the immobilization of lipase on porous structures, which is essential for the economic application of enzymes. Running the adsorption experiment at different temperatures and studying the kinetics of adsorption would provide a better understanding of the adsorption process.

Author Contributions: Conceptualization, S.A.-Z.; validation, A.A.Q. and S.A.-Z.; formal analysis, A.A.Q. and S.A.-Z.; writing—original draft, A.A.Q. and S.A.-Z.; data curation, A.A.Q. and S.A.-Z.; data interpretation, A.A.Q. and S.A.-Z.; methodology, S.A.-Z.; investigation, S.A.-Z.; funding acquisition, S.A.-Z.; supervision, S.A.-Z.; writing—review and editing, A.A.Q. and S.A.-Z.; project administration, S.A.-Z. All authors have read and agreed to the published version of the manuscript.

Funding: This research was funded by the National Water and Energy Center, United Arab Emirates University (UAEU), grant number 31R211.

Institutional Review Board Statement: Not applicable.

Informed Consent Statement: Not applicable.

Data Availability Statement: Not applicable.

Conflicts of Interest: The authors declare no conflict of interest.

Sample Availability: Samples of the compounds are available from the authors.

References

- Contesini, F.J.; Davanço, M.G.; Borin, G.P.; Vanegas, K.G.; Cirino, J.P.G.; Melo, R.R.D.; Mortensen, U.H.; Hildén, K.; Campos, D.R.; Carvalho, P.D.O. Advances in recombinant lipases: Application in the pharmaceutical industry. *Catalysts* **2020**, *10*, 1032. [[CrossRef](#)]
- Kirana, S.; Arshada, Z.; Nosheenb, S.; Kamala, S.; Gulzara, T.; Majeeda, M.S.; Jannata, M.; Rafiquec, M.A. Microbial Lipases: Production and Applications: A Review. *J. Biochem. Biotechnol. Biomater.* **2016**, *1*, 7–20.
- Nguyen, H.H.; Kim, M. An Overview of Techniques in Enzyme Immobilization. *Appl. Sci. Converg. Technol.* **2017**, *26*, 157–163. [[CrossRef](#)]
- Jesionowski, T.; Zdarta, J.; Krajewska, B. Enzyme immobilization by adsorption: A review. *Adsorption* **2014**, *20*, 801–821. [[CrossRef](#)]
- Show, P.-L.; Ling, T.-C.; Lan, J.C.-W.; Tey, B.-T.; Ramanan, R.N.; Yong, S.-T.; Ooi, C.-W. Review of Microbial Lipase Purification Using Aqueous Two-phase Systems. *Curr. Org. Chem.* **2015**, *19*, 19–29. [[CrossRef](#)]
- Sankaran, R.; Show, P.L.; Yap, Y.; Lam, H.L.; Ling, T.C.; Pan, G.-T.; Yang, T.C.-K. Sustainable approach in recycling of phase components of large scale aqueous two-phase flotation for lipase recovery. *J. Clean. Prod.* **2018**, *184*, 938–948. [[CrossRef](#)]
- Hasan, F.; Shah, A.A.; Javed, S.S.; Hameed, A. Enzymes used in detergents: Lipases. *Afr. J. Biotechnol.* **2010**, *9*, 4836–4844.
- Hu, Y.; Dai, L.; Liu, D.; Du, W.; Wang, Y. Progress & prospect of metal-organic frameworks (MOFs) for enzyme immobilization (enzyme/MOFs). *Renew. Sustain. Energy Rev.* **2018**, *91*, 793–801. [[CrossRef](#)]
- Grela, A.; Kuc, J.; Bajda, T. A Review on the Application of Zeolites and Mesoporous Silica Materials in the Removal of Non-Steroidal Anti-Inflammatory Drugs and Antibiotics from Water. *Materials* **2021**, *14*, 4994. [[CrossRef](#)]
- Singh, B.K.; Kim, Y.; Kwon, S.; Na, K. Synthesis of Mesoporous Zeolites and Their Opportunities in Heterogeneous Catalysis. *Catalysts* **2021**, *11*, 1541. [[CrossRef](#)]
- Yang, C.; Wang, Y.; Alfutimie, A. Comparison of Nature and Synthetic Zeolite for Waste Battery Electrolyte Treatment in Fixed-Bed Adsorption Column. *Energies* **2022**, *15*, 347. [[CrossRef](#)]
- Cheng, T.-H.; Sankaran, R.; Show, P.L.; Ooi, C.W.; Liu, B.-L.; Chai, W.S.; Chang, Y.-K. Removal of protein wastes by cylinder-shaped NaY zeolite adsorbents decorated with heavy metal wastes. *Int. J. Biol. Macromol.* **2021**, *185*, 761–772. [[CrossRef](#)] [[PubMed](#)]
- Martínez-Sánchez, J.A.; Arana-Peña, S.; Carballares, D.; Yates, M.; Otero, C.; Fernandez-Lafuente, R. Immobilized Biocatalysts of Eversa® Transform 2.0 and Lipase from Thermomyces Lanuginosus: Comparison of Some Properties and Performance in Biodiesel Production. *Catalysts* **2020**, *19*, 738. [[CrossRef](#)]
- Al-Harby, N.F.; Albahly, E.F.; Mohamed, N.A. Kinetics, Isotherm and Thermodynamic Studies for Efficient Adsorption of Congo Red Dye from Aqueous Solution onto Novel Cyanoguanidine-Modified Chitosan Adsorbent. *Polymers* **2021**, *13*, 4446. [[CrossRef](#)] [[PubMed](#)]
- Ho, Y.S.; Porter, J.F.; McKay, G. Equilibrium Isotherm Studies for the Sorption of Divalent Metal Ions onto Peat: Copper, Nickel and Lead Single Component Systems. *Water Air Soil Pollut.* **2002**, *141*, 1–33. [[CrossRef](#)]
- Saadi, R.; Saadi, Z.; Fazaeli, R.; Fard, N.E. Monolayer and multilayer adsorption isotherm models for sorption from aqueous media. *Korean J. Chem. Eng.* **2015**, *32*, 787–799. [[CrossRef](#)]
- El-Naas, M.H.; Al-Rub, F.A.; Ashour, I.; al Marzouqi, M. Effect of competitive interference on the biosorption of lead (II) by *Chlorella vulgaris*. *Chem. Eng. Process.* **2007**, *46*, 1391–1399. [[CrossRef](#)]
- Subramanyam, B.; Das, A. Linearised and non-linearised isotherm models optimization analysis by error functions and statistical means. *J. Environ. Health Sci. Eng.* **2014**, *12*, 92. [[CrossRef](#)]
- Gurses, A.; Doğar, Ç.; Yalcin, M.; Açıkyıldız, M.; Bayrak, R.; Karaca, S. The adsorption kinetics of the cationic dye, methylene blue, onto clay. *J. Hazard. Mater.* **2006**, *131*, 217–228. [[CrossRef](#)]
- Rahman, M.M.; Shafiullah, A.Z.; Pal, A.; Islam, M.A.; Jahan, I.; Saha, B.B. Study on optimum IUPAC adsorption isotherm models employing sensitivity of parameters for rigorous adsorption system performance evaluation. *Energy* **2021**, *14*, 7478. [[CrossRef](#)]

21. Liu, J.; Wang, X. Novel Silica-Based Hybrid Adsorbents: Lead(II) Adsorption Isotherms. *Sci. World J.* **2013**, *2013*, 897159. [[CrossRef](#)]
22. Sivarajasekar, N.; Baskar, R. Adsorption of Basic Magenta II onto H₂SO₄ activated immature *Gossypium hirsutum* seeds: Kinetics, isotherms, mass transfer, thermodynamics and process design. *Arab. J. Chem.* **2019**, *12*, 1322–1337. [[CrossRef](#)]
23. Mailer, A.R. Chemistry and quality of olive oil. *Prime Facts* **2006**, *227*, 1–4.
24. Khanday, W.A.; Majid, S.A.; Shekar, S.C.; Tomar, R. Dynamic adsorption of DMMP over synthetic zeolite-Alpha. *Arab. J. Chem.* **2014**, *7*, 115–123. [[CrossRef](#)]
25. Byrappa, K.; Kumar, B.V.S. Characterization of zeolites by infrared spectroscopy. *Asian J. Chem.* **2007**, *19*, 4933–4935.
26. Asefa, M.T.; Feyisa, C.B. Comparative Investigation on Two Synthesizing Methods of Zeolites for Removal of Methylene Blue from Aqueous Solution. *Int. J. Chem. Eng.* **2022**, *2022*, 9378712. [[CrossRef](#)]
27. Jamalluddin, N.A.; Abdullah, A.Z. Low frequency sonocatalytic degradation of Azo dye in water using Fe-doped zeolite Y catalyst. *Ultrason. Sonochem.* **2014**, *21*, 743–753. [[CrossRef](#)]
28. Farhan, S.N.; Khadom, A.A. Biosorption of heavy metals from aqueous solutions by *Saccharomyces cerevisiae*. *Int. J. Ind. Chem.* **2015**, *6*, 119–130. [[CrossRef](#)]
29. Rodríguez-estupiñán, P.; Giraldo, L.; Carlos, J. Adsorption calorimetry onto activated carbons prepared from corncobs waste from toluene solutions. *J. Therm. Anal. Calorim.* **2019**, *2*, 2577–2595. [[CrossRef](#)]
30. Tzabar, N.; ter Brake, H.J.M. Adsorption isotherms and Sips models of nitrogen, methane, ethane, and propane on commercial activated carbons and polyvinylidene chloride. *Adsorption* **2016**, *22*, 901–914. [[CrossRef](#)]
31. Yao, G.; Liu, Y.; Zheng, S.; Xu, Y. High removal efficiency of diatomite-based X zeolite for Cu²⁺ and Zn²⁺. *Materials* **2021**, *14*, 6525. [[CrossRef](#)] [[PubMed](#)]
32. Ansari, M.; Raisi, A.; Aroujalian, A.; Dabir, B.; Irani, M. Synthesis of Nano-NaX Zeolite by Microwave Heating Method for Removal of Lead, Copper, and Cobalt Ions from Aqueous Solution. *J. Environ. Eng.* **2015**, *141*, 04014088. [[CrossRef](#)]
33. Tutar, H.; Yilmaz, E.; Pehlivan, E.; Yilmaz, M. Immobilization of *Candida rugosa* lipase on sporopollenin from *Lycopodium clavatum*. *Int. J. Biol. Macromol.* **2009**, *45*, 315–320. [[CrossRef](#)] [[PubMed](#)]
34. Zeng, H.-Y.; Liu, X.-Y.; He, P.; Peng, D.-H.; Fan, B.; Xia, K. Lipase adsorption on woven nylon-6 membrane: Optimization, kinetic and thermodynamic analyses. *Biocatal. Biotransform.* **2014**, *32*, 188–197. [[CrossRef](#)]
35. Wang, F.; Nie, T.T.; Shao, L.L.; Cui, Z. Comparison of physical and covalent immobilization of lipase from *Candida antarctica* on polyamine microspheres of alkylamine matrix. *Biocatal. Biotransform.* **2014**, *32*, 314–326. [[CrossRef](#)]
36. Shomal, R.; Du, W.; Al-Zuhair, S. Immobilization of Lipase on Metal-Organic frameworks for biodiesel production. *J. Environ. Chem. Eng.* **2022**, *10*, 107265. [[CrossRef](#)]
37. Gilani, S.L.; Najafpour, G.D.; Moghadamnia, A.; Kamaruddin, A.H. Kinetics and isotherm studies of the immobilized lipase on chitosan support. *Int. J. Eng. Trans. A Basics* **2016**, *29*, 1319–1331.
38. Rodrigues, A.R.; Cabral, J.M.; Taipa, M. Immobilization of *Chromobacterium viscosum* lipase on Eudragit S-100: Coupling, characterization and kinetic application in organic and biphasic media. *Enzyme Microb. Technol.* **2002**, *31*, 133–141. [[CrossRef](#)]
39. Chen, G.-J.; Kuo, C.-H.; Chen, C.-I.; Yu, C.-C.; Shieh, C.-J.; Liu, Y.-C. Effect of membranes with various hydrophobic/hydrophilic properties on lipase immobilized activity and stability. *J. Biosci. Bioeng.* **2012**, *113*, 166–172. [[CrossRef](#)]
40. Atyaksheva, L.F.; Kasyanov, I.A.; Ivanova, I.I. Adsorptive Immobilization of Proteins on Mesoporous Molecular Sieves and Zeolites. *Pet. Chem.* **2019**, *59*, 327–337. [[CrossRef](#)]
41. Rodhi, M.N.M.; Hamzah, F.; Hamid, K.H.K. Kinetic Behaviour of Pancreatic Lipase Inhibition by Ultrasonicated *A. malaccensis* and *A. subintegra* Leaves of Different Particle Sizes. *Bull. Chem. React. Eng. Catal.* **2020**, *15*, 818–828. [[CrossRef](#)]
42. Bai, Y.-X.; Li, Y.-F.; Yang, Y.; Yi, L.-X. Covalent immobilization of triacylglycerol lipase onto functionalized novel mesoporous silica supports. *J. Biotechnol.* **2006**, *125*, 574–582. [[CrossRef](#)] [[PubMed](#)]
43. Kandasamy, R.; Kennedy, L.J.; Vidya, C.; Boopathy, R.; Sekaran, G. Immobilization of acidic lipase derived from *Pseudomonas gessardii* onto mesoporous activated carbon for the hydrolysis of olive oil. *J. Mol. Catal. B Enzym.* **2010**, *62*, 58–65. [[CrossRef](#)]
44. Dossat, V.; Combes, D.; Marty, A. Efficient lipase catalyzed production of a lubricant and surfactant formulation using a continuous solvent-free process. *J. Biotechnol.* **2002**, *9*, 117–124. [[CrossRef](#)]
45. Maceiras, R.; Vega, M.; Costa, C.; Ramos, P.; Márquez, M. Effect of methanol content on enzymatic production of biodiesel from waste frying oil. *Fuel* **2009**, *88*, 2130–2134. [[CrossRef](#)]
46. Del Pozo, D.F.; van Hauwermeiren, D. Effect of Mass Transfer Limitations on Enzymatic Reactions in Microreactors: A Model-Based Analysis. Master’s Thesis, Ghent University, Ghent, Belgium, 2015.
47. Knezevic, Z.; Mojovic, L.; Adnadjevic, B. Palm oil hydrolysis by lipase from *Candida cylindracea* immobilized on zeolite type Y. *Enzyme Microb. Technol.* **1998**, *22*, 275–280. [[CrossRef](#)]